November 2006

Vacancy Self-trapping During Rapid Thermal Annealing of Silicon Wafers

Thomas A. Frewen
University of Pennsylvania

Talid Sinno
University of Pennsylvania, talid@seas.upenn.edu

Postprint version. Published in *Applied Physics Letters*, Volume 89, Issue 19, Article 191903, November 2006, 3 pages.

Vacancy Self-trapping During Rapid Thermal Annealing of Silicon Wafers

Abstract
The density and spatial distribution of oxide precipitates within a crystalline silicon wafer is of paramount importance for microelectronic device yield. In this letter, the authors show how the formation of previously unconsidered, very small vacancy aggregates can explain macroscopic spatial variations in the oxide precipitate density, which are observed following certain rapid thermal annealing conditions. The formation of these nanometer-sized voids is predicted on the basis of their recent model for vacancy aggregation that accounts for high temperature entropic effects.

Comments
Postprint version. Published in *Applied Physics Letters*, Volume 89, Issue 19, Article 191903, November 2006, 3 pages.

Vacancy self-trapping during rapid thermal annealing of silicon wafers

Thomas A. Frewen[a] and Talid Sinno[b]
Department of Chemical and Biomolecular Engineering, University of Pennsylvania, Philadelphia, Pennsylvania 19104

(Received 20 June 2006; accepted 21 September 2006; published online 6 November 2006)

The density and spatial distribution of oxide precipitates within a crystalline silicon wafer is of paramount importance for microelectronic device yield. In this letter, the authors show how the formation of previously unconsidered, very small vacancy aggregates can explain macroscopic spatial variations in the oxide precipitate density, which are observed following certain rapid thermal annealing conditions. The formation of these nanometer-sized voids is predicted on the basis of their recent model for vacancy aggregation that accounts for high temperature entropic effects. © *2006 American Institute of Physics*. [DOI: 10.1063/1.2385069]

The distribution of oxide precipitates (also known as bulk microdefects or BMDs) within a crystalline silicon wafer is of paramount importance for microelectronic device yield. While oxide precipitates are harmful if present in the near-surface device active region, they provide a critical metal gettering function in the wafer bulk.[1,2] Oxygen precipitates also provide mechanical toughness, which is important for thermal annealing of large-diameter wafers.

It is now well established that under most commercially relevant conditions, oxide precipitation is strongly dependent on the presence of single vacancies, which lower the thermodynamic cost of forming compressively stressed precipitates.[3,4] It has been elegantly demonstrated that relatively straightforward manipulation of vacancy populations by rapid thermal annealing (RTA) of Czochralski-grown wafers can be used to precisely tailor the distribution of oxide precipitates in order to create a "denuded zone" near the wafer surface (corresponding to low vacancy concentration) while producing a high precipitate density in the wafer bulk (high vacancy concentration).[5,6] This profile results from the combination of point defect diffusion to and from the wafer surface and point defect recombination in the wafer bulk. Following RTA, regions of the wafer that have a residual vacancy concentration above a critical value, $C_V^* \sim (1-3) \times 10^{12}$ cm^{-3}, exhibit rapid formation of oxide precipitate nuclei in subsequent nucleation-growth thermal treatments.[5,7]

Recently, RTA experiments under certain annealing protocols, namely, high temperatures and cooling rates, demonstrated unusual BMD density distributions in which the maximum BMD density is observed to lie somewhere in between the wafer edge and the center, leading to a so-called *m*-like profile.[8] Given the importance of BMD density distributions in silicon technology, we specifically address this density variation here by applying a recently developed model for defect diffusion and aggregation.[9]

The approach taken in this work is to first consider the predictions from a point defect-only model and then analyze the effects of including vacancy aggregation. In both cases, it will be assumed that the local BMD density following a nucleation-growth anneal is closely related to the local vacancy concentration at the beginning of the anneal.[5,7] In other words, the BMD density is not explicitly considered but rather implicitly modeled via the vacancy distribution. In the point defect picture, only the diffusion and recombination of self-interstitials and vacancies are considered explicitly, so that

$$\frac{\partial C_I}{\partial t} = \nabla \cdot (D_I(T) \nabla C_I) - k_{IV}(C_I C_V - C_I^{\mathrm{eq}}(T) C_V^{\mathrm{eq}}(T)), \quad (1)$$

$$\frac{\partial C_V}{\partial t} = \nabla \cdot (D_V(T) \nabla C_V) - k_{IV}(C_I C_V - C_I^{\mathrm{eq}}(T) C_V^{\mathrm{eq}}(T)), \quad (2)$$

where D_X and C_X^{eq} are the diffusivities and equilibrium concentrations of species X $(X=I,V)$, respectively, and k_{IV} is the recombination rate. Equilibrium conditions are imposed at the wafer surface.

There exists a long history of investigations aimed at elucidating silicon point defect diffusion coefficients and equilibrium concentrations for use in continuum models of defect dynamics; see Refs. 10 and 11 for reviews. The parameter values used in this work are taken, without any further adjustments, from Ref. 9. These parameters have been obtained using a multimodel, multiexperiment regression study in which experimental data were employed from several sources, including denuded zone depth measurements, oxidation-induced stacking-fault ring dynamics, zinc diffusion profile measurements, and void size and density measurements.[7,12] As discussed in Ref. 7, each of these experimental measurements influenced different aspects of the point defect parameter set, leading to a highly constrained, robust property database. Any changes in any of these properties in the present work would likely destroy one or more of the previous models' ability to reproduce experimental measurements. The relevant parameters are summarized here for convenience:

$$D_I(T) = 0.237 \exp\left(-\frac{0.937}{kT}\right) \mathrm{cm}^2/\mathrm{s}, \quad (3)$$

$$D_V(T) = 7.87 \times 10^{-4} \exp\left(-\frac{0.457}{kT}\right) \mathrm{cm}^2/\mathrm{s}, \quad (4)$$

$$C_I^{\mathrm{eq}}(T) = 2.97 \times 10^{23} \exp(7.67) \exp\left(-\frac{4.0}{kT}\right) \mathrm{cm}^{-3}, \quad (5)$$

[a]Present address: Department of Chemical Engineering, Princeton University, Princeton, NJ 08544.
[b]Author to whom correspondence should be addressed; electronic mail: talid@seas.upenn.edu

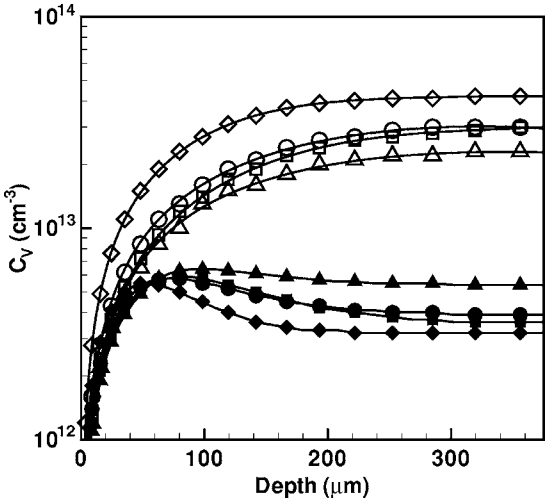

FIG. 1. Vacancy concentration profiles as a function of depth from the wafer surface for several RTA annealing schedules. Open symbols—point defects only: (a) Diamonds—$T_{\text{hold}}=1300\ ^\circ\text{C}$, CR=70 °C/s. (b) Circles—$T_{\text{hold}}=1280\ ^\circ\text{C}$, CR=70 °C/s. (c) Squares—$T_{\text{hold}}=1300\ ^\circ\text{C}$, CR=50 °C/s. (d) Triangles—$T_{\text{hold}}=1280\ ^\circ\text{C}$, CR=50 °C/s. Filled symbols—vacancy aggregation included.

$$C_V^{\text{eq}}(T) = 4.97 \times 10^{22} \exp(7.6) \exp\left(-\frac{3.7}{kT}\right) \text{cm}^{-3}. \qquad (6)$$

The predicted vacancy concentration as a function of depth from the wafer surface for several RTA anneals is shown in Fig. 1 (open symbols). For these simulations, the annealing hold temperature ($T_{\text{hold}}=1280$ or 1300 °C) was applied for 60 s, following by cooling at a constant rate (CR=70 °C/s or 50 °C/s) to 860 °C. The 60 s anneal was sufficient to allow both self-interstitial and vacancy concentrations to reach steady-state (and equilibrium) values at the holding temperature. In all cases, the model predicts a maximum vacancy concentration at the center of the wafer, which is a consequence of vacancy outdiffusion to the wafer surface. On the other hand, a previous study has demonstrated that some combinations of point defect diffusion and equilibrium concentration parameters do, in fact, produce *m*-like vacancy profiles in which the maximum is not located at the wafer center.[8] However, in order to achieve this, the point defect equilibrium concentrations were chosen to have almost identical activation energies and preexponential coefficients, leading to the unlikely constraint that the equilibrium concentrations of self-interstitials and vacancies are within a few percent of each other across several decades.

Here, we propose instead that the formation of very small nanometer-sized voids or *noids* is at least partially responsible for the observed BMD density distribution following RTA. To investigate this possibility, we now include vacancy aggregation into the model represented by Eqs. (1) and (2). Details of the aggregation physics and associated parameters are given in Ref. 9. An important feature of the model is the incorporation of cluster configurational entropy, which has been neglected in previous descriptions.[13] It was shown that cluster configurational entropy lowers the free energy of formation of vacancy clusters, leading to lower supersaturation thresholds for vacancy aggregation and more rapid aggregation kinetics. Shown in the lower half of Fig. 1 (filled symbols) are the vacancy profiles following the same RTA steps as before but now with vacancy aggregation included explicitly. Interestingly, *m*-like profiles are now observed in close agreement with experimental observations,[8] whereby the region with the highest residual vacancy concentration following recombination with self-interstitials exhibits the earliest onset of aggregation during cooling and therefore the *lowest* final vacancy concentration after the RTA treatment. The parametric constraints derived in our previous work[7,9] notwithstanding the present predictions are quite robust with respect to the point defect properties in Eqs. (3)–(6), as long as an excess vacancy concentration is established throughout the wafer following point defect recombination.

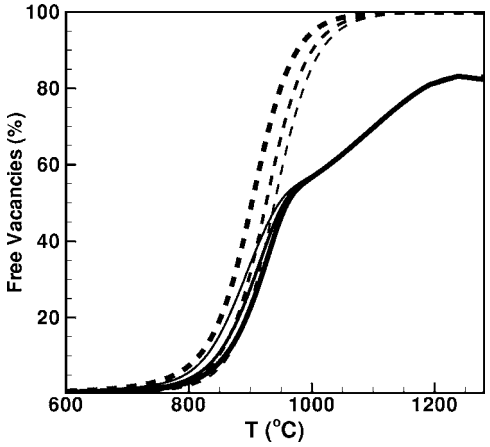

FIG. 2. Solid lines—$V_1=V_{\text{free}}/(V_{\text{free}}+V_{\text{agg}})$, dashed lines—$V_2=V_{\text{free}}/(V_{\text{free}}+V_{\text{O}})$. $T_{\text{hold}}=1280\ ^\circ\text{C}$, CR=70 °C/s. Total oxygen=6×10^{17} cm^{-3}.

Next, the interplay between noid formation and vacancy trapping into OV and/or O_2V complexes was investigated. These complexes are thought to be the building blocks for BMDs in Czochralski silicon wafers.[5] The model in Eqs. (1) and (2) was extended to include reversible reactions between vacancies and oxygen,[7] $V+O_i \leftrightarrow OV+O_i \leftrightarrow O_2V$, in addition to vacancy aggregation. The temperature dependent equilibrium concentrations of the OV and O_2V complexes, along with the single vacancy properties, determine what fraction of the vacancy population is bound into these relatively immobile complexes at any given temperature.[7] The oxygen binding temperature (T_{bind}), defined as the temperature below which at least 50% of the single vacancy population is complexed, is therefore a function of the V, OV, and O_2V formation energies. In the present study, we employ the formation energies computed in Ref. 14. However, the preexponential coefficients, which also are required to fully specify the equilibrium concentrations of OV and O_2V, are not well characterized and are taken here as adjustable parameters in a sensitivity analysis.

The temperature evolutions of the vacancy fractions contained in aggregates, $V_1=V_{\text{free}}/(V_{\text{free}}+V_{\text{agg}})$, and oxygen complexes, $V_2=V_{\text{free}}/(V_{\text{free}}+V_{\text{O}})$, at the wafer center are shown in Fig. 2 for three different oxygen binding temperatures, 900, 925, and 950 °C. These temperatures are in the vicinity of experimental estimates for the binding temperature.[6,7] Note that the oxygen binding temperature is not an absolute quantity; it is coupled to the aggregation physics (and the total oxygen concentration) and is somewhat shifted downwards from what it would be in the absence of vacancy aggregation. As the oxygen complex formation temperature increases (dashed lines shift to the right), noid formation is reduced as shown by the shallower drop in V_1 below 950 °C (solid lines shift to the left).

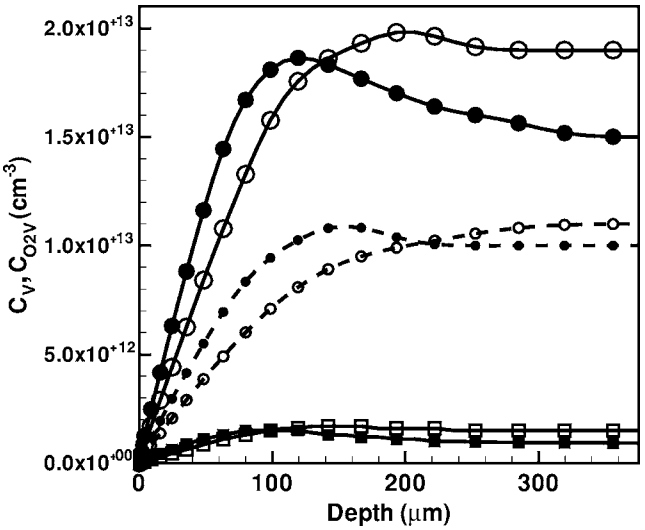

FIG. 3. O_2V concentrations (circles) at 800 °C (large symbols) and 900 °C (small symbols) and V (squares) concentrations for two RTA simulations: T_{hold}=1280 °C (filled symbols) and T_{hold}=1260 °C (open symbols). CR =70 °C/s for both simulations.

The concentrations of free and complexed vacancies (O_2V) during two different RTA treatments are shown in Fig. 3. The free vacancy m-profile shape induces a corresponding m profile in the O_2V concentration by the end of both RTA simulations, at which point $T<T_{bind}$ and O_2V is the dominant species. In other words, in both cases, the majority of the vacancies, whether bound or free, are distributed in an m-like profile by the end of the RTA process. The still-evolving O_2V concentrations at 900 °C during the cooling phase also are shown in Fig. 3. Note that the m shape has not yet developed in the T_{hold}=1260 °C RTA simulation because the vacancy aggregation process is still active, highlighting the coupling between vacancy complexation with oxygen and aggregation.

The noid size distributions at two wafer-depth positions are shown in Fig. 4 for the RTA simulations in Fig. 3. In both cases, the concentration and average size are substantially higher at the wafer center than at a depth of 100 μm, reflecting earlier onset of aggregation at the wafer center. The average noid in the T_{hold}=1280 °C simulation is about 2.75 nm in diameter and contains $\sim 10^3$ vacancies, but is somewhat smaller ($\sim$1.75 nm) in the T_{hold}=1260 °C simulation, where the starting vacancy concentration is lower. Note that in both cases, the noid density is of the same order as the experimentally measured BMD density.[8]

In summary, a mechanism is presented for the formation of spatial variations in the BMD distribution in silicon wafers following RTA treatment. It is proposed that these variations arise from the formation of very small voids, which unfortunately are difficult to observe directly. In addition to altering the spatial distribution of BMDs, it is interesting to note the possibility that the small voids predicted here could themselves act as heterogeneous sites for oxide precipitation, providing another mechanism for BMD formation. It is notable that these predictions are made on the basis of point defect properties that previously have been constrained by regression to multiple independent experiments, which further strengthens the conclusions presented here.

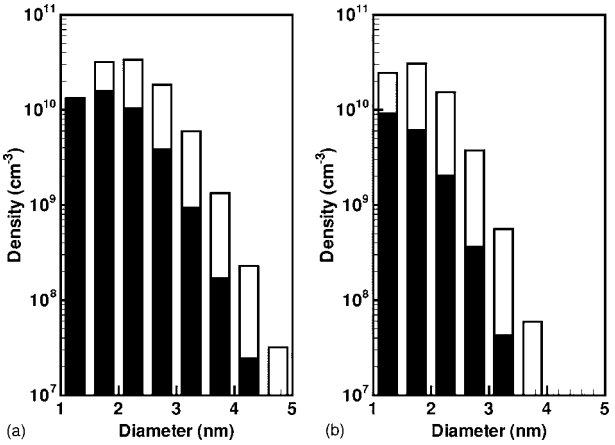

FIG. 4. Void size distribution at wafer center (open bars) and 100 μm (filled bars) for (a) T_{hold}=1280 °C and (b) T_{hold}=1260 °C. CR=70 °C/s for both simulations.

This work was supported by a NSF CAREER Award (CTS01-34418) and Siltronic AG.

[1] R. Falster, G. R. Fisher, and G. Ferrero, Appl. Phys. Lett. **59**, 809 (1991).
[2] G. Kissinger, T. Grabolla, G. Morgenstern, H. Richter, D. Gräf, J. Vanhellemont, U. Lambert, and W. von Ammon, J. Electrochem. Soc. **146**, 1971 (1999).
[3] J. Vanhellemont, J. Appl. Phys. **78**, 4297 (1995).
[4] G. Kissinger, J. Vanhellemont, G. Obermeier, and J. Esfandyari, Mater. Sci. Eng., B **73**, 106 (2000).
[5] R. Falster, V. V. Voronkov, and F. Quast, Phys. Status Solidi B **222**, 219 (2000).
[6] R. Falster and V. V. Voronkov, Mater. Sci. Eng., B **73**, 87 (2000).
[7] T. A. Frewen, T. Sinno, W. Haeckl, and W. von Ammon, Comput. Chem. Eng. **29**, 713 (2005).
[8] M. Akatsuka, M. Okui, N. Morimoto, and K. Sueoka, Jpn. J. Appl. Phys., Part 1 **40**, 3055 (2001).
[9] T. A. Frewen, S. S. Kapur, W. Haeckl, W. von Ammon, and T. Sinno, J. Cryst. Growth **279**, 258 (2005).
[10] T. Sinno, Proc.-Electrochem. Soc. **PV2002-2**, 212 (2002).
[11] T. Sinno, E. Dornberger, R. A. Brown, W. von Ammon, and F. Dupret, Mater. Sci. Eng., R. **R28**, 149 (2000).
[12] T. A. Frewen, T. Sinno, E. Dornberger, R. Hoelzl, W. von Ammon, and H. Bracht, J. Electrochem. Soc. **150**, 673 (2003).
[13] S. Kapur, M. Prasad, J. C. Crocker, and T. Sinno, Phys. Rev. B **72**, 014119 (2005).
[14] M. Pesola, J. von Boehm, T. Mattila, and R. M. Nieminen, Phys. Rev. B **60**, 11449 (1999).